

SPLITTING CRACKS IN REINFORCED CONCRETE ELEMENTS UNDER TENSILE LOADS

B. Tork, J. Gálvez, J. Planas and M. Elices,
Departamento de Ciencia de Materiales, E.T.S.I. Caminos,
Universidad Politécnica de Madrid,
Spain

Abstract

Relative slip between ribbed steel bars and concrete produces radial cracks in reinforced concrete elements subjected to tensile forces. Bond stress is directly related to this cracking through a complex mechanism involving loss of confinement of the bar. Ribbed bar geometry, concrete fracture properties and concrete cover are some of the governing parameters which control the bond capacity. However, a model describing accurately the complex mechanisms involved is still lacking. This paper presents the results of an experimental research to study cracking in prismatic concrete specimens with an embedded ribbed steel bar subjected to tension. The tests were developed for two bar diameters and three concrete covers. The work was carried out in response to the invitation of the "Round Robin Analysis and Tests on Bond" of RILEM TC 147-FMB (1995).

Keywords: Bond, reinforced concrete, deformed bars, slip, tensile load, cracking, fracturing, splitting

1 Introduction

To maintain strain compatibility in reinforced concrete, the bond between the reinforcement and the surrounding concrete must be

guaranteed. However, no accurate model exists to describe the complex mechanisms involved (Noghabai, 1995).

Some bonding actions are caused by chemical adhesion and friction, which are predominantly restricted to bond in plain bars, and their contribution in the case of deformed bars is often negligible. The transfer of force between a ribbed bar and the surrounding concrete is achieved principally by the bearing of the ribs on the concrete. The resultant compressive force exerted by the rib on the concrete is an inclined force. The radial component of this force creates a ring tension in the concrete cover around the bar, Fig. 1 (Tepfers, 1973). If the tension force generated by the bond action exceeds the capacity of the ring, bond failure occurs by splitting of the concrete cover. If the cover is larger or if sufficient confinement opposes the splitting force, a pull-out type failure develops with the concrete being sheared in front of the bar ribs. Splitting type failure, being the weaker mode, is of primary concern for design (Cairns and Jones, 1995).

In recent years, higher steel and concrete strengths have resulted in a trend to design smaller and more congested structural members, with closely-spaced bars near the surface, and the cover is likely to split. Also in many practical applications (Gambarova et al, 1989), such as in short anchorage with limited or no transverse pressure, in lapped splices with limited transverse reinforcement, and at the heads of prestressed, pretensioned thin-webbed beams, concrete is particularly sensitive to splitting because of the wedging action which follows high bond stresses, and which may trigger (through the local collapse of the bond) the collapse of the whole element. In this regard, a better knowledge of all the aspects of splitting is necessary since it is favored by many new materials and new technologies. The aim of this work is to supply experimental results which can help to model bond failure by splitting.

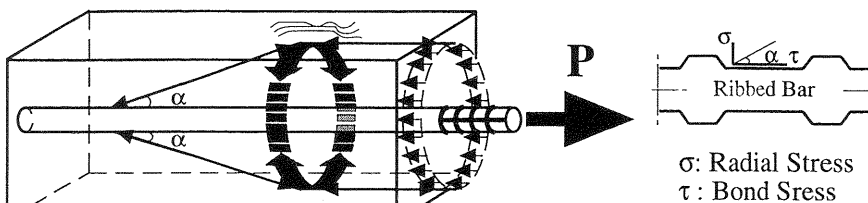


Fig. 1. Tensile stress rings

Materials and specimens

To manufacture the specimens, three identical concrete mixtures of Normal Strength Concrete (NSC) were used, composed of Portland cement, siliceous sand as fine aggregates and siliceous crushed coarse aggregates of 10 mm maximum size. The cement was supplied in bulk to guarantee the homogeneity of the mix. The water/cement ratio was 0.52. The mean settlement with Abram's cone for the three mixtures was 80 mm approximately. The concrete mixtures are shown in Table 1. They were designed to give 30 MPa of compression strength after 28 days.

For each mixture; five prismatic beams (100x100x430 mm) were cast for the fracture energy test, four cylinders (ϕ 75x150 mm) for the compression and the Young's modulus tests, and four cylinders (ϕ 75x150 mm) for the splitting tensile test. The fracture energy was determined in accordance with RILEM three-point bend tests of notched beams (50-FMC), the compressive strength according to ASTM C39, the Young's modulus according to ASTM C469 and the tensile strength according to ASTM C496. Mechanical properties of the concrete are given in Table 2.

The steel of the ribbed bars is grade 500, of Young's modulus (E) 210 GPa, and the yield stress (σ_y) 630 MPa.

The specimens selected for the experimental work were of two different bar diameters (ϕ): one of 8 mm with a cover of 2ϕ and one of 16 mm with covers of 1ϕ , 2ϕ and 3ϕ in accordance with the specifications of the

Table 1. Concrete dosification.

Component	Dosification kg/m ³	Mix Proportion by Weight
Cement	429	1.00
Water	223	0.52
Sand	929	2.16
Coarse Aggregate	730	1.70

Table 2. Mechanical properties of concrete after five months

Mix no.	f_{ck} MPa	f_{ct} MPa	E GPa	G_c N/m
1	35	3.0	28	108
2	35	3.0	28	108
3	36	3.2	28	114

Round Robin invitation (RILEM TC 147-FMB, 1995). Fig. 2 shows the specimen geometry. The dimensions are given in Table 3.

The specimens were cast horizontally in one layer. The moulds were vibrated 12 seconds on a vibrating table. The specimens were left in the moulds 24 hours, covered with saturated sacking at room temperature, and then immersed in lime-saturated water at room temperature until testing. The ends of the bars were covered with waterproof paint. The specimens were tested five months after casting.

The specimen nomenclature is the following: Mixture number.Bar diameter.Cover.Specimen number. For example, the denomination A1.8.C2.3 corresponds to mixture 1, bar diameter 8 mm, cover 2 ϕ and specimen number 3 of these characteristics.

3 Experimental procedure

The tests were performed in displacement control. The velocity of the actuator of the testing machine was 0.03 and 0.12 mm/min for ϕ 8 and ϕ 16 respectively up to the yielding plateau of the steel, and until the end of the test 0.12 and 0.48 mm/min for ϕ 8 and ϕ 16 respectively.

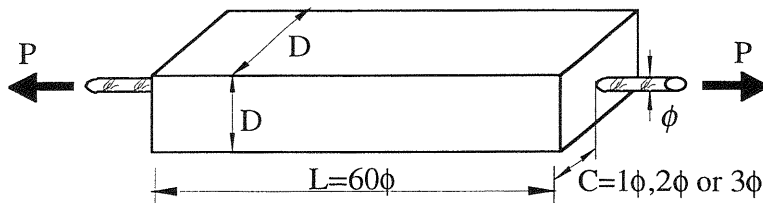


Fig. 2. Specimen geometry

Table 3. Tested specimens

Specimen	Bar Diam., ϕ mm	Length, L mm	Width, D mm	N ^o of Specimens
8.C2	8	480	40	8
16.C1	16	960	48	3
16.C2	16	960	80	5
16.C3	16	960	112	3

The parameters registered during the tests are the following:

- Tensile load P in the bar (Fig. 2).
- Displacement of the actuator of the testing machine.
- Relative displacement between upper and lower faces of the prismatic specimen.
- Relative slip between the steel bar and the upper and lower faces of the concrete, recorded for the initial section of the bar placed on the planes of the faces.
- Opening of the cracks radial to the bar on the upper face of the specimen.

Fig. 3a shows the arrangement of the test and the position of the devices to record the selected parameters. Fig. 3b shows the device used to measure the relative displacement between the bar and the concrete. The crack pattern of the 6 faces of the specimen was drawn after testing.

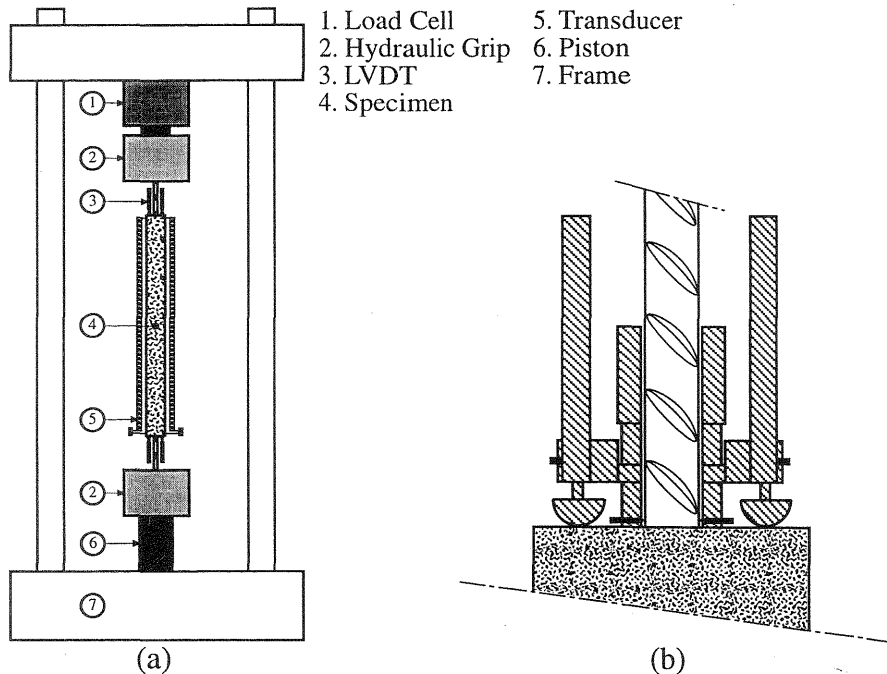


Fig. 3. Test setup: (a) sketch of the specimen in the testing machine, and (b) detail of the device measuring the relative slip between steel bar and concrete

4 Testing equipment

The tests were made on a servocontrolled INSTRON 1275 testing machine, with hydraulic INSTRON clamps to fasten the bars. The load was measured with 100 kN and 1000 kN load cells with $\pm 0.5\%$ error at full scale. INSTRON extensometers, with ± 2.5 mm nominal displacement and ± 0.15 percent error at full scale, were used to measure the COD of the radial cracks and the relative displacement between the upper and lower faces of the prismatic specimen. HBM inductive transducers, with ± 1.0 mm nominal displacement and ± 0.1 percent error at full scale, were used to measure the relative displacement between the bar and the upper and lower faces of the prismatic specimen.

5 Results and discussion

Fig. 4 shows the curves of load P versus relative displacement of the upper and lower faces of the prismatic specimen, for specimens of bar $\phi 16$ with covers 1, 2 and 3 times the diameter. The gauge length was 960 mm. In every group of specimens the point of stiffness reduction coincides

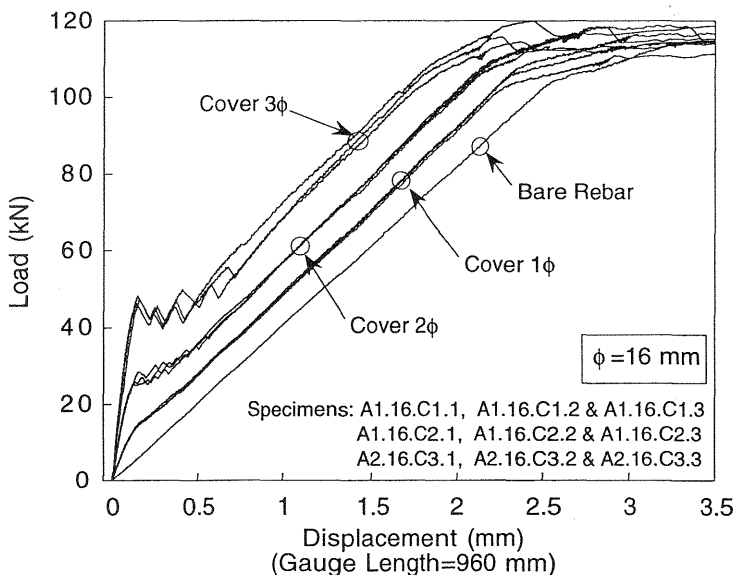


Fig. 4. Load P versus longitudinal displacement curves for specimens with $\phi 16$ bar with 1 ϕ , 2 ϕ , and 3 ϕ cover.

with the appearance of the first transversal crack. The specimens with 2ϕ and 3ϕ covers then show a saw-tooth plateau, each tooth coinciding with the unstable propagation of a transversal crack. When the crack pattern is complete, the tangential stiffness of the specimen is similar to that of the bare bar. The experimental scatter is very narrow.

Fig. 5 shows the curves of mean tensile stress versus mean strain for two specimens with 2ϕ cover, one with $\phi 8$ bar and the other with $\phi 16$ bar. The results are similar, and in both cases the stress at which the sudden reduction of the specimen stiffness occurs is the same. This means that for the same cover, the effect of the bar diameter is small.

Fig. 6 shows the curves of load P versus the relative slip of steel bar and concrete on the upper face of the prismatic specimens with $\phi 16$ bar. The initial parts of the curves are similar for every cover, but the propagation of the cracks produces relaxation of the stresses in the concrete and then the reduction of the relative bar-concrete displacement; so the smaller covers lead to more horizontal curves. Fig. 7 shows the same curves for specimens with $\phi 8$ bar.

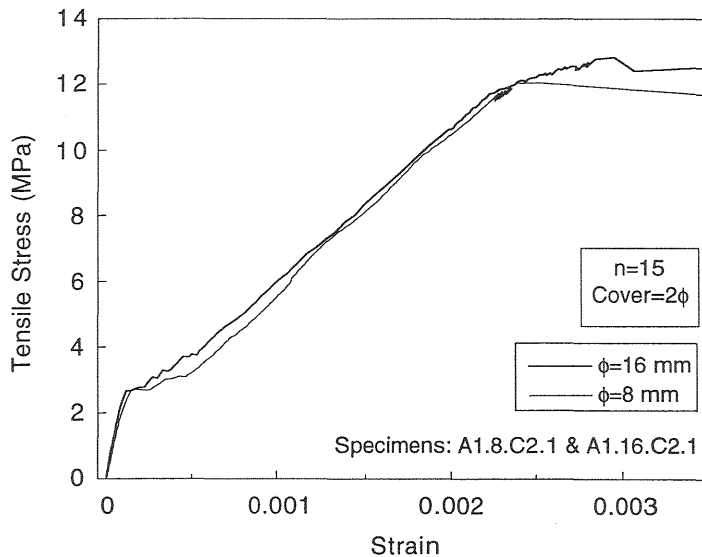


Fig. 5. Stress versus strain curves for specimens with $\phi 16$ and $\phi 8$, both with a 2ϕ cover.

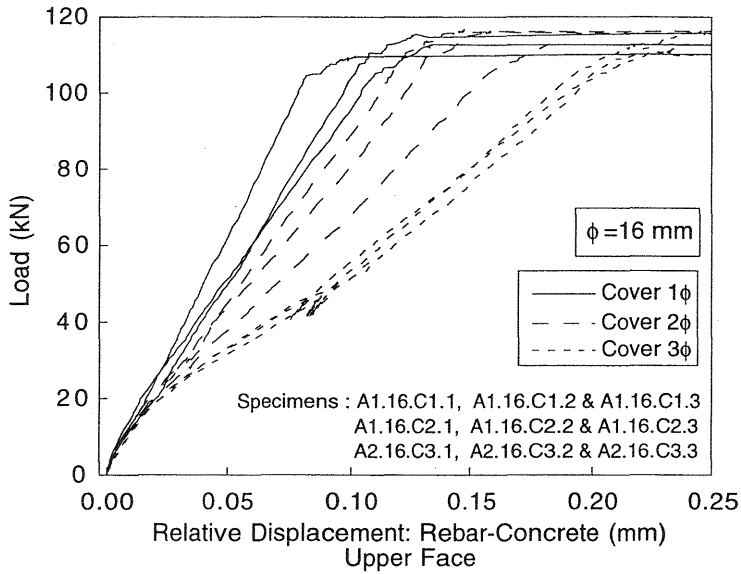


Fig. 6. Load P versus upper face bar-concrete relative displacement curves for specimens with $\phi 16$ bar with 1 ϕ , 2 ϕ , and 3 ϕ cover.

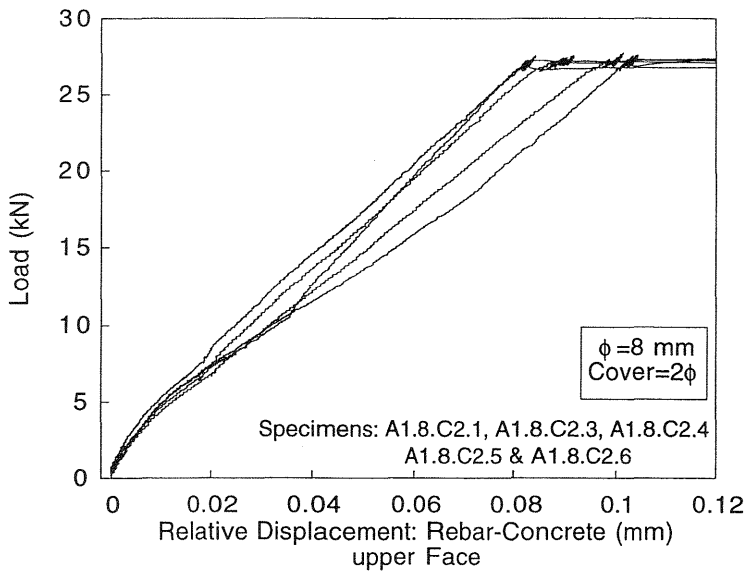


Fig. 7. Load P versus upper face bar-concrete relative displacement curves for specimens with $\phi 8$ bar with 2 ϕ cover.

Fig. 8 shows the curves of load P versus a crack opening displacement (COD) of the radial crack for specimens with $\phi 16$ bar and 2ϕ cover. The square cross-section leads to two groups of cracks almost perpendicular to each other and to the vertical face of the prismatic specimen; sometimes partial radial cracking occurs, and after testing, only one, two or three cracks are visible. Fig. 8 shows the measurements registered by the COD extensometers in both directions, with and without cracks. The first part of the curves, until the break point, is the elastic branch; the break point, in the curves of the specimens with radial cracks captured by the COD extensometers, coincides with the appearance of the first transverse crack (26.5 kN approximately).

Fig. 9 shows the crack pattern on a specimen side. The transversal cracks are perpendicular to the main stress and almost equidistant. The radial cracks follow the shortest paths to the free edges, from the bar

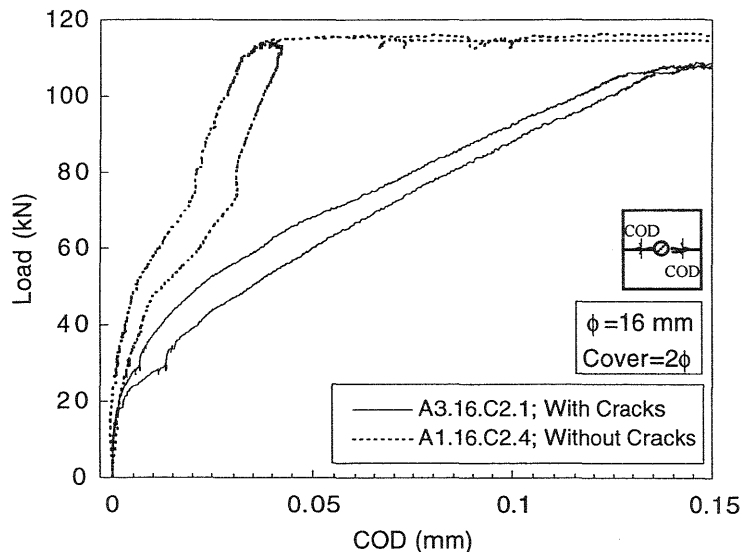


Fig. 8. Load P versus radial crack opening displacement for specimens with $\phi 16$ bar with 2ϕ cover.

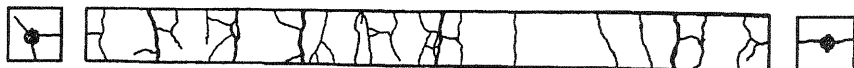


Fig. 9. Crack pattern of a specimen side.

outwards, and from the upper and lower faces to the inside of the specimen. This is important in the numerical simulation because it does not admit two-dimensional analysis.

6 Conclusions

A very important decrease of stiffness coincides with the appearance of the first transversal crack in the specimen. The later transversal cracks grow in an unstable manner, first in the upper part of the specimen and then in the lower part. The transversal cracks are almost equidistant and perpendicular to the main stress. When every transversal crack has grown, the tangential stiffness of the specimen is very close to that of the bare bar.

The radial cracks grow outward from the bar and from the upper and lower faces to the interior of the specimen, showing a very clear 3-D behaviour. They stop when a transversal crack breaks their path.

7 References

- Cairns, J., Jones, K. (1995) The Splitting Forces Generated by Bond. **Magazine of Concrete Research**, 47, 153-165.
- Gambarova, P., Rosati, G., Zasso, B. (1989) Steel-to-Concrete Bond after Concrete Splitting: Constitutive Laws and Interface Deterioration. **Materials and Structures**, 22, 347-356.
- Noghabai, K. (1995) **Splitting of Concrete in the Anchoring Zone of Deformed Bars: A Fracture Mechanics Approach**. Licentiate Thesis, Luleå University of Technology, Publication 95:26L, Luleå, Sweden.
- RILEM TC 147-FMB (1995) **Round Robin Analysis and Tests on Bond-Invitation**. Cachan, Paris.
- Tepfers, R. (1973) **A Theory of Bond Applied to Overlapped Tensile Reinforcement Splices for Deformed Bars**. Chalmers University of Technology, Division of Concrete Structures, Goteborg, Sweden.